Acta Materialia 105 (2016) 16–24

Contents lists available at ScienceDirect

Acta Materialia

journal homepage: www.elsevier.com/locate/actamat

Full length article

Operando reduction of elastic modulus in (Pr, Ce)$O_{2-\delta}$ thin films

Jessica G. Swallow [a, b], Jae Jin Kim [a, b], Mukul Kabir [c], James F. Smith [d], Harry L. Tuller [a, b], Sean R. Bishop [a, b], Krystyn J. Van Vliet [a, b, *]

[a] Department of Materials Science and Engineering, Massachusetts Institute of Technology, 77 Massachusetts Avenue, Cambridge 02139, MA, USA
[b] Materials Processing Center, Massachusetts Institute of Technology, Cambridge 02139, MA, USA
[c] Department of Physics, Indian Institute of Science Education and Research, Pune 411008, India
[d] Micro Materials Ltd., Wrexham LL13 7YL, UK

ARTICLE INFO

Article history:
Received 10 August 2015
Received in revised form
20 November 2015
Accepted 2 December 2015
Available online 24 December 2015

Keywords:
Chemomechanical coupling
Fuel cell materials
Nanoindentation
Mechanical properties (high-temperature deformation)
Cerium oxide (CeO_2)

ABSTRACT

Non-stoichiometric oxides are key functional materials within technologies such as solid oxide fuel cells (SOFCs) and gas sensors that often exhibit interdependent electrochemical and mechanical properties affecting *operando* mechanical stability. Here, we explore this electrochemomechanical coupling experimentally and computationally for (Pr, Ce)$O_{2-\delta}$ (PCO), a model SOFC cathode material. We quantified Young's elastic modulus E of PCO thin films *in situ*, at temperatures up to 600 °C and oxygen partial pressures pO_2 down to 10^{-3} atm via environmentally controlled nanoindentation. The observed significant reduction (up to 40%) in E with increased temperature or decreased pO_2 correlated with changes in oxygen vacancy concentration δ and lattice parameter a expected due to chemical expansion. We confirmed the trend of decreased E with increased δ and a via first principles calculations for bulk PCO. The experimentally observed decrease in E vs. pO_2 and temperature was more extreme than predicted by bulk computations, and is anticipated from the higher concentration of vacancies in thin films relative to bulk. These results demonstrate that accurate models of deformation in thin-film devices comprising these chemomechanically coupled oxides may differ markedly from bulk counterparts, and must reflect significant, reversible decreases in elastic moduli resulting from increased temperature and decreased pO_2.

1. Introduction

Non-stoichiometric oxides are an important class of functional materials for energy related technologies including solid oxide fuel cells (SOFCs), permeation membranes, and automotive emission gas sensors. Their prevalence in these applications is attributable to the capacity for both electronic and ionic conductivity enabled by their defect chemistry, and high-temperature stability, to serve as device electrodes and to support mixed ionic-electronic conduction (MIEC). SOFC devices often operate in extreme temperature and oxygen partial pressure (pO_2) conditions, exposing, for example, the oxides comprising the cathode to 300–1000 °C and pO_2 varying from 0.2 (oxidizing in air) to $<10^{-3}$ (reducing) atm, the latter under polarized conditions. New oxides and device designs are under consideration for SOFCs, aimed to reduce operation temperatures and start-up times and to increase mechanical durability, including use of thin film non-stoichiometric oxides as electrodes. Given that such materials have been shown to exhibit strong correlation between the electrochemical and mechanical states (electrochemomechanical coupling [1–3]), and that such coupling may provide means to tailor electrochemical properties such as conductivity as a function of mechanical strain [4–8], the *in situ* mechanical properties of such oxides are of interest. In particular, accurate predictions of both material and device performance depend on whether and how the elastic moduli of such films depend on temperature and pO_2, or can be predicted from analysis of bulk non-stoichiometric oxides.

Many non-stoichiometric electrode materials undergo significant dilation upon release of oxygen, termed chemical expansion, during exposure to reducing conditions typical for SOFCs. Empirical and first principles calculations have demonstrated that chemical expansion arises from two competing factors: expansion from the increased diameter of reduced cations, and contraction around

* Corresponding author. Laboratory for Material Chemomechanics (8-237), Massachusetts Institute of Technology, 77 Massachusetts Avenue, Cambridge 02139, MA, USA.
E-mail address: krystyn@mit.edu (K.J. Van Vliet).

http://dx.doi.org/10.1016/j.actamat.2015.12.007
1359-6454/

oxygen vacancies [9–13]. Several researchers have also found evidence for mechanical failure originating from fracture in SOFC electrodes due to thermochemical expansion mismatch of materials. For example, Sato et al. attributed this failure to tensile stresses that arise in the SOFC cathode initiated from chemical expansion of the ceria-based anode cell support, based on their analysis of bulk oxides that included acoustic emission analysis, post-mortem inspection, and finite element modeling [14,15]. When mechanical properties vary with electrochemical state, this coupling is termed electrochemomechanics. Knowledge of *operando* electrode and electrolyte mechanical properties, including the Young's elastic modulus E, can facilitate predictions of how such stresses will develop in the functional materials and within multimaterial devices to improve mechanical durability of functional oxide layers.

(Pr, Ce)$O_{2-\delta}$ (PCO) is a model functional oxide for such applications. This fluorite structured oxide undergoes large changes in non-stoichiometry δ and corresponding oxygen vacancy concentration in both cathodic and anodic SOFC conditions, along with significant chemical expansion [2,16,17]. Large changes of δ in cathodic conditions are facilitated by the ease of Pr reduction, and thus larger volume fractions of Pr within the oxide generally increase electrochemical reducibility in these conditions [18]. Due to the mixed-valent nature of Pr, PCO is a mixed ionic-electronic conductor under relatively oxidizing conditions [3,19]. It is known that Pr reduction within PCO is accompanied by both an increased oxygen vacancy concentration, as described in Kröger-Vink notation in Eq. (1), and an increased lattice parameter a in PCO [18,19]:

$$2Pr_{Ce}^{\times} + O_O^{\times} \leftrightarrow 2Pr'_{Ce} + V_O^{\bullet\bullet} + \frac{1}{2}O_{2(g)} \quad (1)$$

Here, $Pr_{Ce}^{\times}$ and Pr'_{Ce} denote Pr^{4+} and Pr^{3+}, respectively, on Ce sites, $O_O^{\times}$ denotes O^{2-} on an oxygen site, and $V_O^{\bullet\bullet}$ denotes a vacancy on an oxygen site. The elastic constants of vacancy-free ceria have been computed by density functional theory [20]. For Pr-doped CeO_2, vacancy formation and migration energies have been estimated via density functional theory (DFT) and kinetic Monte Carlo simulations [21–23]. However, it is not yet established whether Pr reduction results in detectable and significant changes in the elastic modulus of (Pr, Ce)$O_{2-\delta}$.

Although to our knowledge there have been no previous reports on *in situ* elastic properties of (Pr, Ce)$O_{2-\delta}$ thin films, there have been prior *in situ* and *ex situ* studies on bulk forms of related functional oxides. For example, others have shown that bulk oxides such as (Gd, Ce)$O_{2-\delta}$ (Gd-doped ceria, or GDC), (La, Sr) (Co, Fe)$O_{3-\delta}$ (LSCF), and $Y_{0.15}Zr_{0.85}O_{2-\delta}$ (YSZ) exhibit lattice expansion that is correlative with elastic properties [24–27]. Amezawa et al. found by acoustic emission that an increase in lattice parameter, due to either chemical or thermal expansion, led to a decrease in the elastic modulus E in bulk GDC [24]. This trend has been replicated with molecular dynamics simulations using interatomic potentials [28,29]. Together, these studies suggest that Pr reduction could lead to a decrease in E of PCO, directly influencing how stress will develop in oxide components subjected to elevated temperatures or oxygen partial pressure gradients [25,30]. However, few studies have explored how such expansion may impact mechanical properties of thin films, particularly *in situ* and in contrast to bulk counterparts [31]. Thin films may differ from bulk oxides in the extent of such coupling between electrochemical reduction and mechanical properties, due to the influence of strain at the film–substrate interface, the potential for vacancy concentrations higher than in bulk due to space charge effects at surfaces and grain boundaries, and the possibility of anisotropic expansion resulting from a clamped geometry [32–34].

Here we quantified the elastic modulus of $Pr_{0.2}Ce_{0.8}O_{2-\delta}$ (PCO) thin films via *in situ* nanoindentation under controlled temperature (24–600 °C) and oxygen partial pressure (pO_2 of 0.2–7.6 × 10^{-4} atm), to approximate *operando* conditions of SOFCs. High temperature nanoindentation has been demonstrated as a technique for measuring mechanical properties of bulk and thin film samples at temperatures up to 700 °C for diverse material classes including oxides and alloys [35–37]. We correlated these results with oxygen vacancy concentration via a point defect and chemical expansion model developed previously for bulk PCO [2,3,18], and compared these experimental findings with our predictions based on DFT calculations of elastic constants for bulk compositions. Due to the challenges associated with nanoscale mechanical measurements at such elevated temperatures, we included statistical analysis to identify significant changes in E as a function of composition, temperature, or pO_2 [38]. Together, these results demonstrated that E decreased significantly with increasing lattice parameter a. This increase in a was concurrent with increased oxygen vacancy concentrations quantified by the non-stoichiometry parameter δ, which was modulated by increased temperature and decreased pO_2. The magnitude of E for PCO thin films was lower than that predicted for bulk PCO counterparts, and the lattice expansion-associated reduction in E of these Pr-doped CeO_2 thin films also significantly exceeded that reported for bulk Gd-doped CeO_2 [24].

2. Methods

2.1. Sample preparation

Films of undoped CeO_2 and $Pr_{0.2}Ce_{0.8}O_{2-\delta}$ were deposited by pulsed laser deposition (PLD) onto (001) oriented single crystal YSZ (8 mol% Y_2O_3 stabilized zirconia) substrates (10 × 5 × 0.5 mm^3; MTI Corporation, Richmond, CA) using dense targets prepared by sintering the corresponding powders above 1400 °C under N_2 atmosphere [39]. After reaching the base pressure (8.5 × 10^{-6} Torr), substrates were heated to ~ 250 °C. A Coherent (Santa Clara, CA) COMPex Pro 205 KrF eximer laser, emitting at a wavelength of 248 nm, was used for ablating the target materials with a configuration of 400 mJ/pulse and 10 Hz laser repetition rate. The oxygen pressure was maintained at 10.0 mTorr during both the deposition and the cooling steps. Post-deposition annealing at higher oxygen pressure and deposition temperature, typically performed to ensure complete oxidation, was not conducted in order to avoid rapid changes in the volume of the films that promote cracking. As-prepared films were annealed at 750 °C in air for 1 h. Heating and cooling rates were 2 °C/min.

Film thickness was determined via surface profilometry (KLA-Tencor P-16 + stylus profiler) as 1.09 ± 0.03 μm for the CeO_2 film and 1.11 ± 0.06 μm for the $Pr_{0.2}Ce_{0.8}O_{2-\delta}$ film. X-ray diffraction patterns (XRD; X'Pert PRO MPD, PANalytical) obtained from $2\theta-\omega$ coupled scans of the films exhibited highly (001)-oriented texture. Surface topographic analysis by atomic force microscopy (AFM; Digital Instruments Nanoscope IV) demonstrated dense and smooth films with root-mean-square surface roughness of approximately 0.4 nm, sufficiently smooth for instrumented indentation.

2.2. Elastic modulus measurement via in situ nanoindentation

Elastic moduli for each sample and condition were measured *in situ*, at temperatures ranging from 25 to 600 °C and under oxygen partial pressures ranging from 0.21 – 7.6 × 10^{-4} atm at 600 °C, using an instrumented nanoindenter (MicroMaterials NanoTest Vantage; Wrexham, UK) capable of elevated temperatures and controlled gas environments. Both the sample and the cubic

boron-nitride indenter of Berkovich pyramidal geometry were heated to the same temperature to minimize thermal drift. See Ref. [40] for additional information on high-temperature measurements with this specific indentation instrument. The loading rate was between 0.1 and 0.5 mN/s, with a maximum depth of 100 nm. Depth-dependent trends in elastic moduli were not detectable for indentations below this depth, and thus no finite-thickness correction was applied to account for mechanical contributions from the substrate.

For all conditions, at least four indentation arrays, each of which comprised of at least 25 indentations, were acquired; each array was located at a distinct location on the sample surface spaced at least 60 μm from the nearest adjacent array. Indentations with sufficiently low signal-to-noise ratio, poor indenter contact, excessive (> 100 nm) plastic depth, or pop-ins during loading were excluded from further analysis, resulting in at least four arrays of at least ten indentations for each condition (i.e., four distinct locations with ten replicate experiments at that location, for a total of approximately 40 indentations per sample per condition defined by temperature and pO_2). One condition had fewer total indentations: CeO_2 at 600 °C in 7.6×10^{-3} atm oxygen comprised three arrays of at least 10 indentations each. Indentation center-to-center spacing within each array of 25 was 30 μm to minimize mechanical interactions among indentations.

Gas concentration was controlled by flowing nitrogen and oxygen at a fixed ratio through the indenter chamber, and oxygen partial pressures of the exhaust gas were measured using a custom-built Nernst-type YSZ-based oxygen sensor operated at 620 °C. Heating and cooling rates were 1.6 °C/min to prevent thermal shocking of samples, and a minimum of 12 h were provided for samples and the measurement apparatus to equilibrate at the target temperature and oxygen partial pressure.

Young's elastic modulus E was calculated according to the method of Oliver and Pharr via Eq. (2), where A is the projected contact area of the probe at a given plastic depth h_c that we calculated according to an area function calibrated based on a standard sample of inconel or fused silica $A(h_c)$, and S is the measured unloading stiffness [41].

$$E = \frac{1-\nu^2}{\frac{2\sqrt{A}}{S\sqrt{\pi}} - \frac{1-\nu_i^2}{E_i}} \tag{2}$$

The elastic modulus E_i and Poisson's ratio ν_i of the indenter were assumed as 800 GPa and 0.12, respectively; the Poisson's ratio ν of the CeO_2 and Pr-doped CeO_2 samples was assumed as 0.33, within the range reported previously for acoustic emission measurements of Gd-doped CeO_2 at elevated temperatures [24].

2.3. Statistical analysis of indentation data

One-way analysis of variance (ANOVA) based on Sokal and Rohlf was conducted on the multiple indentation arrays acquired on each sample at each condition, to determine whether these data acquired at four different sample locations could be considered to come from the same population of data, or if there was detectable variance among the arrays acquired under ostensibly identical conditions [42]. Detailed discussion of the statistical method used to analyze nanoindentation results has been published previously [38], and is summarized briefly as follows. Three metrics of statistical comparison were computed (p-value < 0.05, Tukey–Kramer minimum significant difference, and Gabriel's comparison interval); if at least two of these three showed that there was significant variance among indentation arrays for a given sample and condition, then the grand mean of the arrays was reported with standard error for n representing the number of arrays. Otherwise, the arithmetic mean of all indentations for a given sample condition was reported, with standard error reported for n as the number of indentations. Such array-to-array variance could be attributable to variations in sample topography or composition at different locations on the sample surface, variations in temperature of the contacting probe and sample at different sample locations, or variations in indenter geometry acquired during indentation among multiple arrays. The function describing probe geometry $A(h_c)$ was calibrated immediately prior to and following data acquisition for each condition, to minimize contributions from this latter source of variance.

2.4. Calculation of non-stoichiometry parameter and lattice parameter

Oxygen non-stoichiometry parameters δ for (Pr, Ce)$O_{2-\delta}$ were calculated based on the defect model for bulk PCO outlined by Bishop et al. [18] Lattice parameters a were estimated according to Eq. (3) based on the value of the lattice parameter a_o of undoped CeO_2 and $Pr_{0.2}Ce_{0.8}O_{2-\delta}$ reported at room temperature (5.41 Å [43,44]), the thermal expansion coefficient of ceria α_T (1.2×10^{-5} K^{-1} [45]), and the chemical expansion coefficient of PCO α_C (0.087 [2]). The chemical expansion coefficient α_c, analogous to α_T, relates $\Delta\delta$ to chemical strain ε_c. This approach assumes that in the oxidized case the PCO lattice parameter can be approximated by that of CeO_2, since Pr^{+4} and Ce^{+4} are nearly the same size (0.96 and 0.97 Å radii, respectively) [46]. Our own density functional theory calculations described below support this assumption. The reference vacancy concentrations δ_{ref} were values calculated by the defect model at room temperature (10^{-16} for CeO_2 and 10^{-7} for $Pr_{0.2}Ce_{0.8}O_{2-\delta}$).

$$a = a_o\left(1 + \alpha_T(T - 298K) + \alpha_C\left(\delta - \delta_{ref}\right)\right) \tag{3}$$

2.5. Density functional theory calculations of lattice parameter and elastic constants

The generalized gradient approximation (GGA) to density functional theory (DFT) with incorporation of the Hubbard U term was used to calculate the lattice parameters and elastic constants of CeO_2 and Pr-doped CeO_2 with varying vacancy concentrations, using the Vienna ab-initio simulation package (VASP) [47–49]. Inclusion of the Hubbard U term accounted for the on-site Coulomb repulsion of the localized 4f electrons in Ce [50,51]. A magnitude of U = 5.0 eV was used for Ce, which has been shown previously to reproduce the chemical expansion coefficient of $CeO_{2-\delta}$ [21,52]. This U overestimates the lattice constant a and Young's modulus of CeO_2 by ~ 1% and ~ 14%, respectively. However, because the chemical expansion coefficient is accurately reproduced by this U, it is expected that trends in ΔE vs. Δa and $\Delta\delta$ will be accurately reproduced for bulk PCO, while the magnitudes of E and a will be systematically overestimated. No U term was included for Pr. The Perdew-Burke-Ernzerhof (PBE) exchange-correlation functional was used with a basis set composed of projected augmented wave (PAW) pseudopotentials, with an energy cutoff of 500 eV [53–55]. A 2 × 2 × 2 (96 atoms) supercell was constructed from conventional unit cells of CeO_2, and Pr and oxygen vacancies were substituted in as needed. Before calculating elastic constants, the lattice parameter and atomic positions of the supercell at each composition were permitted to relax with a 2 × 2 × 2 Monkhorst-Pack k-point grid applied to CeO_2. Elastic constants C_{ij} were then calculated on the relaxed structure. Oxygen vacancy positions were

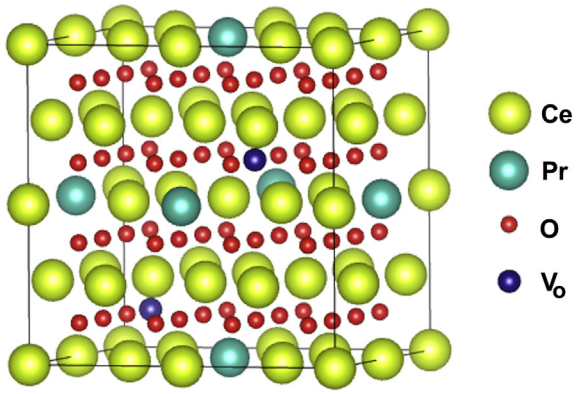

Fig. 1. Schematic of the 2 × 2 × 2 supercell of $Pr_xCe_{1-x}O_{2-\delta}$ used for elastic constant calculation by density functional theory. Cerium atoms (Ce) are large spheres shown in yellow, praseodymium atoms (Pr) are large spheres in green, oxygen atoms (O) are small spheres in red, and oxygen vacancies (V_o) are small spheres in blue. For δ=0.03125 calculations, only one of the vacancies was present, while for the δ=0.0625 calculation, the supercell contained two vacancies. The Pr configuration shown is for the x = 0.09325 calculations; for other values of x these sites were occupied by Ce and Pr was substituted for Ce in other locations in the supercell. Species radii are not to scale.

chosen, as shown in Fig. 1, to be maximally distant because such systems were of minimum system energy at that vacancy concentration. Pr positioning was varied depending on target Pr concentration, and variation of the relative spacing between Pr atoms did not significantly affect lattice parameter or elastic constants.

3. Results

$CeO_{2-\delta}$ and $Pr_{0.2}Ce_{0.8}O_{2-\delta}$ thin films, deposited to ~ 1 μm thickness on (001) YSZ substrates as described in Section 2.1, were highly (001) textured as evidenced by X-ray diffraction and exhibited a root-mean-square surface roughness of < 0.5 nm as measured via atomic force microscopy. This notation for PCO indicates Pr content of $x = 0.2$, and non-stoichiometry parameter δ that varies with the physical environment and resulting oxygen vacancy content.

At room temperature, we previously reported measurement of the Young's elastic modulus E of $CeO_{2-\delta}$ and $Pr_{0.2}Ce_{0.8}O_{2-\delta}$ thin films as 264.6 ± 2.2 GPa and 276.5 ± 7.7 GPa, respectively [38]. These magnitudes are in excellent agreement with other reported values of E for bulk samples measured by nanoindentation in the same conditions for bulk $Pr_{0.2}Ce_{0.8}O_{2-\delta}$ (274 ± 25 GPa [56]) and undoped ceria (264.1 ± 2.2 GPa [25]). At room temperature, therefore, E of these as-deposited thin films matched previously reported bulk values, validating this measurement technique for evaluating the elastic modulus of thin films.

3.1. Elastic moduli under operando temperature and oxygen environments

When the oxygen partial pressure was decreased from 0.2 to 7.6×10^{-4} atm at a constant temperature of 600 °C, E of $Pr_{0.2}Ce_{0.8}O_{2-\delta}$ decreased significantly from ~ 250 GPa–150 GPa (Fig. 2(a)). In fact, this Pr-doped ceria also exhibited statistically significant decreases in E at 600 °C and an intermediate pO_2 of 7.5×10^{-3} atm as compared to room temperature in air. No significant change was identified for $CeO_{2-\delta}$ over this change in atmospheric conditions at 600 °C. According to the defect model of bulk $Pr_xCe_{1-x}O_{2-\delta}$ described by Bishop et al., the above decrease in oxygen partial pressure at 600 °C corresponds to a change in

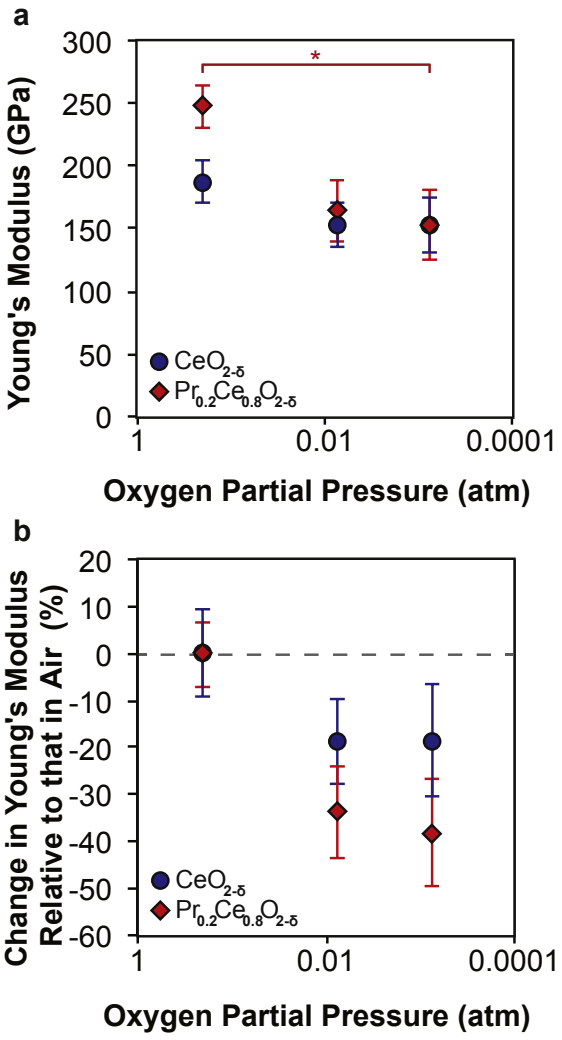

Fig. 2. (a) Young's elastic moduli E of (Pr, Ce)$O_{2-\delta}$ thin films measured *via* nanoindentation at 600 °C. E decreases with decreased oxygen partial pressure at 600 °C. The decrease in E observed for $Pr_{0.2}Ce_{0.8}O_{2-\delta}$ at 7.6×10^{-4} atm pO_2 with respect to air (0.21 atm) is statistically significant with $\alpha < 0.05$ (denoted by bracket marked (*)), while no significant change in E is observed with decreased pO_2 for undoped ceria. Non-bracketed points for the same sample are statistically indistinguishable. (b) The % decrease in E for (Pr, Ce)$O_{2-\delta}$ thin films relative to the value measured for the same composition at 600 °C in air is larger for Pr-doped ceria when the oxygen partial pressure decreases from 0.2 atm to 7.6×10^{-4} atm. For both (a) and (b), error bars are standard error of the mean.

oxygen vacancy content $\Delta\delta$ of 0.04 for $Pr_{0.2}Ce_{0.8}O_{2-\delta}$, and 4×10^{-7} for $CeO_{2-\delta}$ [18].

To facilitate comparison between the undoped and Pr-doped ceria, Fig. 2(b) shows the percentage change in E at 600 °C relative to that measured for the sample of the same composition at that temperature in air. The 38 ± 11% decrease in E observed with reduced oxygen partial pressure for Pr-doped ceria was statistically significant, while the apparent decrease in E observed for ceria upon this pO_2 excursion was not.

3.2. Relation of elastic properties to oxygen vacancy concentration and lattice parameter

This reduction in E of $Pr_{0.2}Ce_{0.8}O_{2-\delta}$ with decreasing pO_2 at constant temperature of 600 °C can be expressed in terms of increasing non-stoichiometry or oxygen vacancy content δ, where

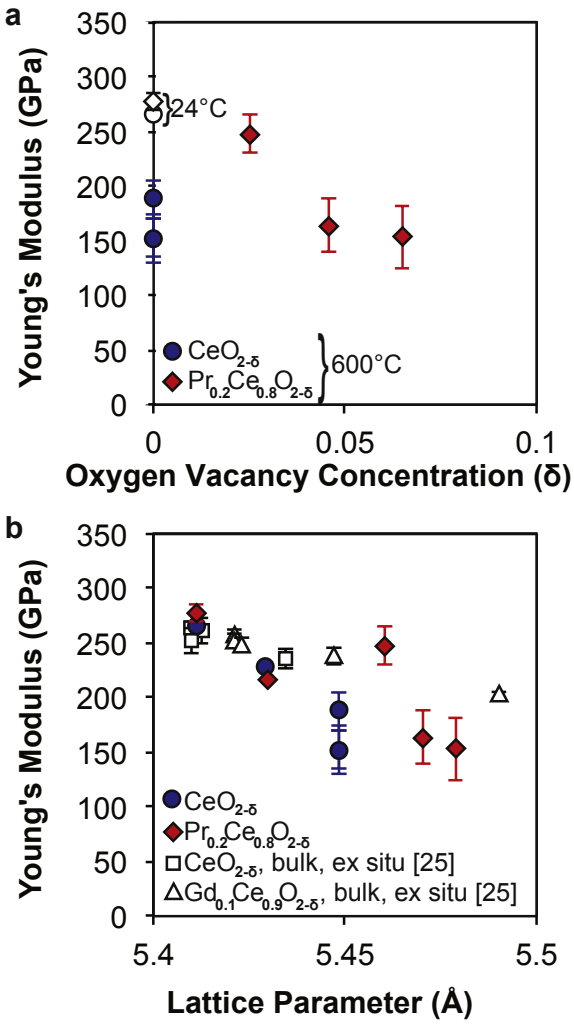

Fig. 3. (a) *In situ* nanoindentation measurements of Young's elastic modulus *E vs.* non-stoichiometry δ of (Pr, Ce)$O_{2-\delta}$ thin films at 600 °C, where δ is increased by decreasing oxygen partial pressure pO_2. Open symbols indicate for reference room temperature measurements from Ref. [38]. Increases in δ associated with decreased pO_2 are more apparent on this scale for $Pr_{0.2}Ce_{0.8}O_{2-\delta}$ and correlate with decreasing *E* because δ is orders of magnitude larger in $Pr_{0.2}Ce_{0.8}O_{2-\delta}$ than in $CeO_{2-\delta}$. (b) *E* decreases with increasing lattice parameter *a*. For $CeO_{2-\delta}$, the change in *E* observed is attributed to thermal expansion as temperature increases. δ is estimated according to the defect model in Ref. [18] and *a* is calculated as described in Section 2.4. For both (a) and (b), error bars are standard error of the mean, and may appear smaller than data points. Shown for comparison are the values of *E* (± standard deviation) reported in Ref. [25] for bulk $CeO_{2-\delta}$ and $Gd_{0.1}Ce_{0.9}O_{2-\delta}$ measured at room temperature in air (*ex situ* conditions) for samples with oxygen vacancy concentration varied by quenching from high temperature.

δ is derived from an established defect model for PCO [18]. Fig. 3a illustrates this reduction in mechanical stiffness with increasing vacancy concentration in $Pr_{0.2}Ce_{0.8}O_{2-\delta}$. Here, open symbols indicate *E* measured at room temperature in air, for reference. Note that δ is several orders of magnitude lower in undoped $CeO_{2-\delta}$ than in $Pr_{0.2}Ce_{0.8}O_{2-\delta}$; thus, increases in δ associated with decreased pO_2 are more apparent on this scale for $Pr_{0.2}Ce_{0.8}O_{2-\delta}$. In contrast to the marked reduction in *E* as a function of pO_2 at 600 °C, undoped ceria did not exhibit statistically distinguishable changes in *E* upon reduced pO_2. In other words, a significant decrease in the magnitude of *E* was found only when the oxygen vacancy content δ was also altered significantly via the environmental conditions, as afforded by the greater reducibility of Pr. This relatively stronger response of PCO to elevated temperature and reduced oxygen partial pressure is not wholly unexpected, in that Pr reduction facilitates a greater increase in vacancy concentration relative to undoped ceria.

This decrease in *E* can also be considered in terms of the lattice parameter *a*, which can increase due to thermal and/or chemical expansion and is determined as a function of coefficients of thermal and chemical expansion and δ (see Section 2.4). Lattice parameter changes with respect to room temperature in air were estimated from a combination of the vacancy content change $\Delta\delta$ coupled to the chemical expansion coefficient of (Pr, Ce)$O_{2-\delta}$ reported in Ref. [2] and the thermal expansion coefficient of $CeO_{2-\delta}$ reported in Ref. [45]. Fig. 3(b) shows that, over the range of lattice parameters resulting from change in temperature and/or oxygen partial pressure, *E* generally decreased with increasing *a* for both ceria and Pr-doped ceria thin films. The effective slope of this *E*(*a*) correlation, in terms of percentage decrease in *E* per 1% increase in lattice parameter, was 42± 10% for undoped ceria and 36± 8% for Pr-doped ceria. Fig. 3(b) also includes, for comparison, the relatively weaker trend of decreased *E* with increased *a* that was reported previously for bulk samples of $CeO_{2-\delta}$ and $Gd_{0.1}Ce_{0.9}O_{2-\delta}$ [25]. Note that those prior measurements of bulk samples were *ex situ*, in that samples were quenched to retain vacancy concentrations and then tested via nanoindentation at room temperature in air [25]. As discussed below, the greater apparent uncertainty in *E* at larger lattice parameters for results in the present study as compared to Ref. [25] arises in part from experimental design differences and from the practical challenges of conducting *in situ* nanoindentation at elevated temperature, though the same trend of decreasing *E* with increasing *a* is apparent.

First principles calculations of elastic constants C_{ij} for bulk ceria and Pr-doped ceria with finite vacancy content also demonstrated a significant reduction in stiffness with increasing lattice parameter associated with increasing δ. Table 1 summarizes computed C_{11} and *E* for three compositions of $CeO_{2-\delta}$ with either zero or finite oxygen vacancy concentration denoted by δ. Generally, a larger δ correlated with increased lattice parameter and decreased *E* and C_{11}. (See Supplementary Fig. S1 and S2 for graphical rendering.) While the magnitudes of *E* calculated via density functional theory (DFT + U) exceeded those determined experimentally, the calculated chemical expansion coefficient of 0.088 (unitless) matched well with the reported experimental value (0.087 [2]); this correlation is expected because the magnitude of the Hubbard U term (see Section 2.5) was optimized for this parameter. The magnitudes of elastic stiffness constants C_{11}, C_{12}, and C_{44} for undoped, vacancy-free $CeO_{2-\delta}$ agreed well with those reported previously by Kanchana et al. for the same system within the generalized gradient approximation (354, 99, and 51 GPa, respectively) [20]. Addition of Pr to the supercell minimally altered the lattice parameter or elastic constants as compared to undoped $CeO_{2-\delta}$ in this vacancy-free case. This is expected given that the Shannon ionic radii of Pr with +3 and + 4 charge (1.126 and 0.96 Å, respectively) are

Table 1
Structural and elastic constants for $Pr_xCe_{1-x}O_{2-\delta}$ calculated by density functional theory.

Pr content *x*	Nonstoichiometry δ	Lattice constant *a* (Å)	C_{11} (GPa)	C_{12} (GPa)	C_{44} (GPa)	*E* (GPa)
0	0	5.48	343	93	54	303
0	0.03125	5.49	332	97	52	288
0	0.0625	5.51	326	100	55	279
0.03125	0	5.48	343	94	51	302
0.0625	0	5.48	341	92	52	301
0.09375	0	5.48	372	122	35	312
0.09375	0.03125	5.49	336	97	55	292

comparable to those of Ce (1.143 and 0.97 Å, respectively) [46]. Therefore, it is expected that the effect of chemical expansion on the elastic constants of Pr-doped and undoped ceria should be comparable.

Further, the trend of this $E(a)$ dependence predicted by these simulations (20% decrease in E per 1% increase in lattice parameter as compared to undoped ceria without vacancies) was similar to that found experimentally for PCO films with appreciable Pr content and δ (36% decrease in E per 1% increase in lattice parameter), but the trend was less pronounced. In fact, the trend predicted by simulation agrees well with that reported in Ref. [25] for experimental measurements on bulk $CeO_{2-\delta}$ (~ 23% decrease in E per 1% increase in a). There are several reasons why the magnitude of E is greater for the simulated bulk oxides as compared to the experimentally measured thin films, as we discuss below. However, the underlying trend and importance of the *operando* conditions to the mechanical stiffness of this functional oxide is clear: E decreased with increasing a, whether the lattice parameter increased by increased temperature and/or increased vacancy content denoted by δ.

4. Discussion

We sought to determine whether and to what extent the elastic properties of PCO thin films may be altered under *operando* conditions known to promote chemical expansion, and found that indeed the elastic moduli of Pr-doped ceria decreased significantly at the high temperatures and low oxygen partial pressures typical of solid oxide fuel cell conditions. In fact, these *in situ* nanoindentation measurements demonstrated that E of undoped ceria and PCO thin films decreased with increasing lattice parameter, driven by both thermal and chemical expansive effects. E was also confirmed to decrease with increasing lattice parameter using DFT computational simulations of bulk counterparts for the same materials and similar non-stoichiometry δ. The decrease in E has been observed previously in bulk samples of ceria-based materials and has been attributed to the weakening of resistance to bond stretching, as bond length increases upon thermochemical expansion [30,57]. The reduction in E per unit increase in lattice parameter was larger for our *in situ* experiments as compared to previous measurements of E for other functional oxides in bulk form, and as compared to our own DFT predictions. These differences may be attributable to several possible factors, relating to both technical aspects of the measurement and unique characteristics of these chemomechanically coupled oxides in thin-film form.

First, we note that *in situ* nanoindentation measurements of thin films at such elevated temperatures and controlled atmospheres include certain technical challenges [35–37]. The uncertainty in measured E was greater at elevated temperatures than at room temperature, as indicated by the standard error of the mean denoted in Fig. 3(a). For this reason, statistical analysis of calculated elastic moduli for each set of samples and conditions was employed to identify significant changes in E as a function of elevated temperature, reduced oxygen partial pressure, and initial composition. The relatively higher variance at extreme temperatures is attributed chiefly to uncertainty in the accuracy of the probe geometric area function (contact area calibrated as a function of contact depth, as discussed below), and to slight differences in absolute temperature at the probe-sample interface for each replicate indentation site acquired over a span of 16–24 h on a given sample surface [35,37]. Results presented herein include only thermally well-matched experiments, meaning that temperature stability was achieved for both the probe and sample in contact, as described in Ref. [58]. Over the extended durations at elevated temperatures required of such experiments that systematically varied pO_2 for a given sample, the boron nitride probe geometry was not invariant. This probe material was selected for its stability at high temperatures, but repeated experiments on standard samples (fused silica after cooling to room temperature, or inconel at elevated temperatures) indicated detectable variations in the contact area relation $A(h_c)$ employed in Eq. (2). Accurate measurement of E does not require that $A(h_c)$ is constant among all sample sets, only that it is known. We determined this function experimentally before and after acquiring each set of indentations at each condition, to minimize contributions to variance in E from changes in probe geometry. However, this variance in measured E motivated detailed statistical analysis to objectively identify significant changes in film stiffness with either temperature or pO_2 (see Section 2.3 and Ref. [38]). Further, although there is potential for degradation of the sample (via cracking or surface contamination upon heating) to affect measured E in such films, these factors did not measurably contribute to the recorded changes in E. Films were deliberately heated and cooled at the slow rate of 1.6 °C/minute to avoid thermochemical expansion induced shock, and no evidence of significant crack concentrations or delamination was observed on post-tested samples by optical microscopy. Additionally, we identified no correlation between changes in elastic moduli and the duration that a sample was exposed to high temperature and/or specific pO_2, as would be consistent with surface contamination. We also did not detect changes in loading curvature or pop-in events that would be indicative of cracking, delamination, or contributions from a surface contaminant in the load-depth hystereses analyzed herein. Thus, such possible contributions to marked reduction in E of PCO at high temperature and low pO_2 appeared minimal. In summary, notwithstanding the technical challenges associated with heating and indenting these ceria-based films that could lead to appreciable variance in mean elastic modulus, the above calibration and control experiments support the primary finding: *operando* elastic modulus of PCO films decreased significantly with increasing non-stoichiometry δ, from ~ 250 GPa in air at room temperature to ~ 150 GPa in ~ 10^{-3} pO_2 at 600 °C.

Second, we can compare these results for PCO thin films to those of related functional oxides in bulk form. As highlighted in Fig. 3(b), *via* nanoindentation Wang et al. reported decreasing E for increasing lattice parameter, for bulk $CeO_{2-\delta}$ and $Gd_{0.1}Ce_{0.9}O_{1.95-\delta}$ (Gd-doped ceria, often termed GDC rather than GCO) at room temperature; in those studies, vacancy concentrations within the room temperature samples were varied by quenching from higher temperatures with correspondingly varying oxidation states [25]. The reported magnitude of E is comparable for the most oxidized of these bulk samples (smallest a) to our own measured E for thin films at room temperature; however, the rate of decrease in E per increase in a (~ 23% decrease in E per 1% increase in a) was weaker than that observed for our thin film samples. This weaker dependence of ΔE as a function of Δa in bulk samples was also reported for GDC under *operando* conditions by Amezawa et al. Those authors quantified E for bulk GDC via acoustic measurements, over a range of temperature and pO_2 that correlated with changes in lattice parameter a [24]. For that bulk oxide, they found that E decreased from 190 GPa to 150 GPa as a increased from ~ 5.42–5.48 Å. In that sense, undoped (bulk and thin film), Gd-doped (bulk) and Pr-doped ceria (thin films analyzed herein) showed decreased stiffness with increased lattice parameter brought on by changes in external physical environment. However, we note that the severity of this change was less pronounced in the bulk GDC over this change in a, with only ~ 10% reduction in E for a 1% increase in lattice parameter. This comparison simply shows that it is reasonable that E decreases with increasing lattice parameter in such functional oxides by 10s of GPa in *operando* conditions, and does not resolve whether the extent of this reduction is attributable

chiefly to differences in composition (dopant species) or sample geometry (bulk or thin film). In principle, both factors can affect the vacancy concentration as a function of physical variables, which in turn affect a and E.

Indeed, the vacancy concentration of PCO thin films typically exceeds bulk counterparts, as we have demonstrated previously [32]. Figure 4 illustrates this in terms of the non-stoichiometry parameter δ for Pr-doped ceria ($Pr_{0.1}Ce_{0.9}O_{2-\delta}$, a different composition than measured here) as a function of oxygen partial pressure at 600 °C. The vacancy content was consistently greater in thin films of < 1 μm thickness as compared to bulk PCO with the same average Pr-content [2,32,59]. Although the full quantification of why such differences in point defect concentrations in non-stoichiometric oxide films and bulk exist is beyond the scope of the current study, it is attributed plausibly to relatively greater contributions of vacancy-rich regions such as the film surface and film–substrate interface regions. More importantly, this established higher concentration of vacancies in thin films is consistent with our finding that E measured for our PCO thin films was lower than that predicted via DFT for bulk PCO counterparts, as discussed further below. Trends with increasing lattice parameter and δ would be expected to hold for predictions and measurements in bulk, though the magnitude of E and the rate of change with respect to δ may appear more pronounced in thin films because the vacancy content predicted by the bulk model underestimates the actual vacancy content of thin films and thus also underestimates the % change in a under a given set of conditions. While the origin of these variations is not fully understood, studies suggest that film/substrate lattice mismatch strain effects and space charge depletion/accumulation of defects near interfaces (e.g., grain boundaries) could play a dominant role in the relatively higher concentration of vacancies in thin films [33,34,60]. Additionally, as PCO is cubic and elastically anisotropic, in these (100) textured films, together the elastic anisotropy and strong texturing of this material may serve as additional sources of variation between indentation-extracted elastic moduli of the bulk and thin film forms.

Finally, we note that thin films may also exhibit lower E relative to bulk counterparts of similar composition due to constrained chemical expansion of the film upon increasing oxygen vacancy content. As in-plane expansion of the adherent thin film is constrained, theoretically the chemical expansion coefficient α_c is amplified out-of-plane (normal to the film–substrate interface) by a factor of $(\nu+1)/(\nu-1)$, where ν is the Poisson's ratio of the film [34]. A typical estimate of ν from bulk measurements of other oxides is ~ 0.33 [24], providing an estimated amplification of out-of-plane chemical expansion in PCO that could range up to twofold. Although this anisotropic expansion cannot be related directly to changes in a and E measured via indentation, we note the tendency for effective a to increase upon such constrained expansion and that $E(a)$ did increase approximately twice as much in experiments on thin films as was reported from previous experiments or predicted via our present DFT calculations for bulk counterparts. This suggests an alternative and perhaps additional mechanism by which E of thin films increases to a greater extent than predicted or measured for bulk counterparts.

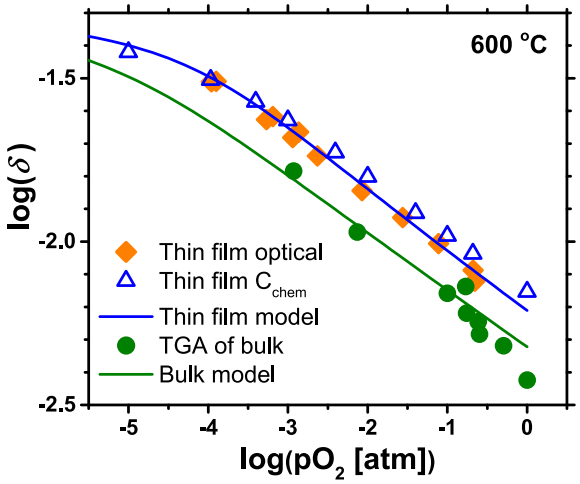

Fig. 4. Vacancy content δ varies in Pr-doped ceria as a function of decreased partial pressure at 600 °C. The vacancy content of thin films is consistently higher than in bulk counterparts of the same volume-averaged composition. Optical data are from Ref. [59], thin film chemical capacitance (C_{chem}) and thin film model data are from Ref. [32], and bulk thermogravimetric analysis (TGA) data and model are from Ref. [2].

Our *ab initio* calculations indicated that differences between bulk and thin film stiffness can be expected for appreciable Pr-content x in such oxides, as a function of vacancy content defined by δ (Table 1 and Supplementary Fig. S1 and S2). Specifically, these DFT results demonstrated that E decreased in these functional oxides with increasing oxygen vacancy content quantified by δ, which in turn increased a. For undoped ceria ($x = 0$), the lattice parameter increased by 0.5% as δ increased from zero (perfect crystal) to 0.06 (comparable to our experimental δ at the lowest pO_2). The effective elastic modulus E decreased by nearly 10% as a result of this vacancy-mediated increase in lattice parameter. In the absence of vacancies and at lower Pr-doping of $x = 0.03$ or 0.06, E was approximately the same as for vacancy-free, undoped ceria. For a fixed Pr-content ($x = 0.09$) but increased vacancy content δ (from 0 to 0.03), however, E decreased from 312 to 292 GPa. If we approximate this dependence $E(a)$ as a negative linear correlation (with least-squares regression $R^2 = 0.95$), overall the dependence $E(a)$ was predicted as ~ 20% reduction in E per 1% increase in lattice parameter as compared to undoped ceria without vacancies. For the Pr-containing compositions, the predicted correlation was slightly more pronounced at 30% reduction in stiffness per 1% increase in a. These dependences were less than the relative decrease in E measured for our thin films (~ 40%), but agreed well with the ~ 23% decrease in E for ~ 1% increase in a reported by Wang et al. for bulk undoped ceria via *ex situ* indentation measurements [25]. Therefore, the trends reported here for DFT computations on PCO are consistent with experimental results on bulk counterparts, and deviations from the present experimental results may be attributable to microstructural differences between bulk and thin film counterparts discussed above. As these *ab initio* simulations predicted the structural and elastic properties of the bulk material (and are not currently feasible via DFT for substrate-adhered thin films of this material at ~ 1 μm thickness), this similar but relatively lower dependence of mechanical stiffness on non-stoichiometry in such predictions may be attributed reasonably to a higher average vacancy content in thin films as compared to bulk oxides with appreciable Pr-content x, in addition to the other thin film factors described above. That expectation is supported by the calculations in which we varied δ for an otherwise constant average composition: even for constant x, an increase in vacancy content defined by δ resulted in an increase in a and corresponding decrease in E. Thus, our DFT results predict trends for E vs. a for doped ceria that compare well with previously reported experimental results for bulk samples, and highlight the role of chemical expansion due to increased δ in modulating E that become even more pronounced in thin films under *operando* conditions.

Taken together, these experiments and calculations demonstrate that thin films of functional oxides such as Pr-doped ceria exhibit significant reduction in mechanical stiffness with increasing oxygen vacancy content, mediated by changes in the lattice parameter a under *operando* conditions. This change is more

pronounced in Pr-doped ceria thin films than in a previous report for bulk Gd-doped ceria under similar conditions, and we attribute this chiefly to the relatively greater vacancy content and effective lattice parameter of thin films as compared with bulk functional oxides of similar dopant content *x*.

5. Conclusions

The Young's elastic modulus *E* of thin films of (Pr, Ce)$O_{2-\delta}$ was measured by nanoindentation at temperatures up to 600 °C, and at 600 °C at oxygen partial pressures between 0.2 and 7.6 × 10^{-4} atm. Per 1% increased lattice parameter, caused by a combination of thermal and chemical expansion, a decrease in *E* of 36%± 8% was observed for PCO. Density functional theory (DFT + U) calculations of bulk counterparts also predicted decreased *E* with increased vacancy concentration and lattice parameter for undoped and Pr-doped $CeO_{2-\delta}$ at several vacancy concentrations; however, DFT predicted this change in *E* at about 20% per 1% change in lattice parameter. The more pronounced decrease in *E* observed for PCO thin films may be attributable to differences between thin films and bulk samples, including increased vacancy concentrations in films due to elevated values of δ at grain boundaries or in space charge regions, or increased lattice parameter in the out-of-plane direction due to constrained expansion. An understanding of how mechanical properties such as elastic modulus of non-stoichiometric oxides are affected by changes in non-stoichiometry caused by temperature or oxygen partial pressure change is highly relevant to predicting where stresses or strains will arise in actual devices comprised of such chemomechanically coupled materials, and thereby facilitate mechanically robust designs. Especially for devices involving thin film components, predicting strain arising due to such coupling enables use of strain to enhance gas reactivity, ionic conductivity, or other functional properties. These findings suggest that elastic properties of thin films change markedly *operando*, and may deviate significantly from bulk counterparts even under the same environmental conditions. Together, these results motivate further *in situ* experimentation and computational modeling for this and other material classes (e.g., perovskites), to refine these predictions for design of non-stoichiometric materials and devices for SOFCs, gas sensors, permeation membranes, and other oxide-enabled applications.

Acknowledgments

This work was supported by the U.S. Department of Energy, Basic Energy Sciences, Division of Materials Science and Engineering under award number DE–SC0002633. J.G. Swallow acknowledges support from the DOE-SCGF Fellowship Program administered by ORISE-ORAU under contract no. DE-AC05-06OR23100. J.J. Kim thanks the Kwanjeong Educational Foundation for fellowship support. M. Kabir acknowledges support from the Department of Science and Technology, India under the Ramanujan Fellowship. We thank J. M. Maloney for valuable discussion of statistical methods and M. Youssef for assistance with density functional theory calculations. This work made use of the Shared Experimental Facilities supported in part by the MRSEC Program of the National Science Foundation under award number DMR-1419807.

Appendix A. Supplementary data

Supplementary data related to this article can be found at http://dx.doi.org/10.1016/j.actamat.2015.12.007.

References

[1] B. Yildiz, "Stretching" the energy landscape of oxides–Effects on electrocatalysis and diffusion, MRS Bull. 39 (2014) 147–156.
[2] S.R. Bishop, H.L. Tuller, Y. Kuru, B. Yildiz, Chemical expansion of non-stoichiometric $Pr_{0.1}Ce_{0.9}O_{2-\delta}$: Correlation with defect equilibrium model, J. Eur. Ceram. Soc. 31 (2011) 2351–2356.
[3] H.L. Tuller, S.R. Bishop, D. Chen, Y. Kuru, J.J. Kim, T.S. Stefanik, Praseodymium doped ceria: Model mixed ionic electronic conductor with coupled electrical, optical, mechanical and chemical properties, Solid State Ionics 225 (2012) 194–197.
[4] E.D. Wachsman, K.T. Lee, Lowering the temperature of solid oxide fuel cells, Science 334 (2011) 935–939.
[5] B.C.H. Steele, A. Heinzel, Materials for fuel-cell technologies, Nature 414 (2001) 345–352.
[6] Y. Chen, Z. Cai, Y. Kuru, W. Ma, H.L. Tuller, B. Yildiz, Electronic activation of cathode superlattices at elevated temperatures- source of markedly accelerated oxygen reduction kinetics, Adv. Energy Mater 3 (2013) 1221–1229.
[7] W. Ma, J.J. Kim, N. Tsvetkov, T. Daio, Y. Kuru, Z. Cai, Y. Chen, K. Sasaki, H.L. Tuller, B. Yildiz, Vertically aligned nanocomposite $La_{0.8}Sr_{0.2}CoO_3/(La_{0.5}Sr_{0.5})_2CoO_4$ cathodes – electronic structure, surface chemistry and oxygen reduction kinetics, J. Mater. Chem. A 3 (2015) 207–219.
[8] H. Jalili, J.W. Han, Y. Kuru, Z. Cai, B. Yildiz, New insights into the strain coupling to surface chemistry, electronic structure, and reactivity of $La_{0.7}Sr_{0.3}MnO_3$, J. Phys. Chem. Lett. 2 (2011) 801–807.
[9] D. Marrocchelli, S.R. Bishop, H.L. Tuller, B. Yildiz, Understanding chemical expansion in non-stoichiometric oxides: Ceria and zirconia case studies, Adv. Funct. Mater 22 (2012) 1958–1965.
[10] S.J. Hong, A.V. Virkar, Lattice parameters and densities of rare-earth oxide doped ceria electrolytes, J. Am. Ceram. Soc. 78 (1995) 433–439.
[11] D. Marrocchelli, N.H. Perry, S.R. Bishop, Understanding chemical expansion in perovskite-structured oxides, Phys. Chem. Chem. Phys. 17 (2015) 10028–10039.
[12] S.R. Bishop, D. Marrocchelli, C. Chatzichristodoulou, N.H. Perry, M.B. Mogensen, H.L. Tuller, E.D. Wachsman, Chemical expansion: Implications for electrochemical energy storage and conversion devices, Annu. Rev. Mater. Res. 44 (2014) 205–239.
[13] S.R. Bishop, D. Marrocchelli, N.H. Perry, H.L. Tuller, G. Watson, B. Yildiz, K. Amezawa, J.A. Kilner, Chemical expansion in SOFC materials: Ramifications, origins, and mitigation, ECS Trans. 57 (2013) 643–648.
[14] K. Sato, K. Yashiro, T. Kawada, H. Yugami, T. Hashida, J. Mizusaki, Fracture process of nonstoichiometric oxide based solid oxide fuel cell under oxidizing/reducing gradient conditions, J. Power Sources 195 (2010) 5481–5486.
[15] K. Sato, H. Omura, T. Hashida, K. Yashiro, H. Yugami, T. Kawada, J. Mizusaki, Tracking the onset of damage mechanism in ceria-based solid oxide fuel cells under simulated operating conditions, J. Test. Eval. 34 (2006) 246–250.
[16] D. Chen, S.R. Bishop, H.L. Tuller, Praseodymium-cerium oxide thin film cathodes: Study of oxygen reduction reaction kinetics, J. Electroceram 28 (2012) 62–69.
[17] R. Chiba, H. Taguchi, T. Komatsu, H. Orui, K. Nozawa, H. Arai, High temperature properties of $Ce_{1-x}Pr_xO_{2-\delta}$ as an active layer material for SOFC cathodes, Solid State Ionics 197 (2011) 42–48.
[18] S.R. Bishop, T.S. Stefanik, H.L. Tuller, Defects and transport in $Pr_xCe_{1-x}O_{2-\delta}$: Composition trends, J. Mater. Res. 27 (2012) 2009–2016.
[19] S.R. Bishop, T.S. Stefanik, H.L. Tuller, Electrical conductivity and defect equilibria of $Pr_{0.1}Ce_{0.9}O_{2-\delta}$, Phys. Chem. Chem. Phys. 13 (2011) 10165–10173.
[20] V. Kanchana, G. Vaitheeswaran, A. Svane, A. Delin, First-principles study of elastic properties of CeO_2, ThO_2 and PoO_2, J. Phys. Condens. Mater 18 (2006) 9615–9624.
[21] P.P. Dholabhai, J.B. Adams, P. Crozier, R. Sharma, Oxygen vacancy migration in ceria and Pr-doped ceria: A DFT+U study, J. Chem. Phys. 132 (2010) 094104.
[22] P.P. Dholabhai, S. Anwar, J.B. Adams, P. Crozier, R. Sharma, Kinetic lattice Monte Carlo model for oxygen vacancy diffusion in praseodymium doped ceria: Applications to materials design, J. Solid State Chem. 184 (2011) 811–817.
[23] K. Ahn, D.S. Yoo, D.H. Prasad, H.-W. Lee, Y.-C. Chung, J.-H. Lee, Role of multivalent Pr in the formation and migration of oxygen vacancy in Pr-doped ceria: Experimental and first-principles investigations, Chem. Mater 24 (2012) 4261–4267.
[24] K. Amezawa, T. Kushi, K. Sato, A. Unemoto, S.-i. Hashimoto, T. Kawada, Elastic moduli of $Ce_{0.9}Gd_{0.1}O_{2-\delta}$ at high temperatures under controlled atmospheres, Solid State Ionics 198 (2011) 32–38.
[25] Y. Wang, K. Duncan, E.D. Wachsman, F. Ebrahimi, The effect of oxygen vacancy concentration on the elastic modulus of fluorite-structured oxides, Solid State Ionics 178 (2007) 53–58.
[26] Y. Kimura, J. Tolchard, M.-A. Einarsrud, T. Grande, K. Amezawa, M. Fukuhara, S.-i. Hashimoto, T. Kawada, Anelastic properties of $La_{0.6}Sr_{0.4}Co_{1-y}Fe_yO_{3-\delta}$ at high temperatures, Solid State Ionics 262 (2014) 337–339.
[27] T. Kushi, K. Sato, A. Unemoto, S. Hashimoto, K. Amezawa, T. Kawada, Elastic modulus and internal friction of SOFC electrolytes at high temperatures under controlled atmospheres, J. Power Sources 196 (2011) 7989–7993.
[28] H. Xu, R.K. Behera, Y. Wang, F. Ebrahimi, S.B. Sinnott, E.D. Wachsman, S.R. Phillpot, A critical assessment of interatomic potentials for ceria with application to its elastic properties, Solid State Ionics 181 (2010) 551–556.

[29] M. Burbano, D. Marrocchelli, B. Yildiz, H.L. Tuller, S.T. Norberg, S. Hull, P.A. Madden, G.W. Watson, A dipole polarizable potential for reduced and doped CeO_2 obtained from first principles, J. Phys.: Condens. Mater 23 (2011) 255402.
[30] K.L. Duncan, Y. Wang, S.R. Bishop, F. Ebrahimi, E.D. Wachsman, Role of point defects in the physical properties of fluorite oxides, J. Am. Ceram. Soc. 89 (2006) 3162–3166.
[31] J.P. Nair, E. Wachtel, I. Lubomirsky, J. Fleig, J. Maier, Anomalous expansion of CeO_2 nanocrystalline membranes, Adv. Mater 15 (2003) 2077–2081.
[32] D. Chen, S.R. Bishop, H.L. Tuller, Non-stoichiometry in oxide thin films: A chemical capacitance study of the praseodymium-cerium oxide system, Adv. Funct. Mater. 23 (2013) 2168–2174.
[33] B.W. Sheldon, S. Mandowara, J. Rankin, Grain boundary induced compositional stress in nanocrystalline ceria films, Solid State Ionics 233 (2013) 38–46.
[34] S.R. Bishop, D. Chen, J. Sheth, S.T. Misture, B.W. Sheldon, J.J. Kim, H.L. Tuller, Impact of size scale on electro-chemo-mechanical coupling properties in MIECs: Bulk and thin film $(Pr,Ce)O_{2-\delta}$, ECS Trans. 61 (2014) 31–36.
[35] R. Ctvrtlik, M.S. Al-Haik, V. Kulikovsky, Mechanical properties of amorphous silicon carbonitride thin films at elevated temperatures, J. Mater. Sci. 50 (2015) 1553–1564.
[36] Z. Huang, A. Harris, S.A. Maloy, P. Hosemann, Nanoindentation creep study on an ion beam irradiated oxide dispersion strengthened alloy, J. Nucl. Mater 451 (2014) 162–167.
[37] M. Rebelo de Figueiredo, M.D. Abad, A.J. Harris, C. Czettl, C. Mitterer, P. Hosemann, Nanoindentation of chemical-vapor deposited Al_2O_3 hard coatings at elevated temperatures, Thin Solid Films 578 (2015) 20–24.
[38] J.G. Swallow, J.J. Kim, S.R. Bishop, J.F. Smith, H.L. Tuller, K.J. Van Vliet, Elasto-plastic properties of $(Pr, Ce)O_{2-\delta}$ thin films, ECS Trans. 68 (2015) 847–855.
[39] J.J. Kim, S.R. Bishop, N. Thompson, Y. Kuru, H.L. Tuller, Optically derived energy band gap states of Pr in ceria, Solid State Ionics 225 (2012) 198–200.
[40] N.M. Everitt, M.I. Davies, J.F. Smith, High temperature nanoindentation- the importance of isothermal contact, Philos. Mag. 91 (2011) 1221–1244.
[41] W.C. Oliver, G.M. Pharr, An improved technique for determining hardness and elastic modulus using load and displacement sensing indentation experiments, J. Mater. Res. 7 (1992) 1564–1583.
[42] R.R. Sokal, F.J. Rohlf, Biometry, W. H. Freeman and Company, New York, NY, 1995.
[43] M. Yashima, D. Ishimura, Y. Yamaguchi, K. Ohoyama, K. Kawachi, High-temperature neutron powder diffraction study of cerium dioxide CeO_2 up to 1770 K, Chem. Phys. Lett. 372 (2003) 784–787.
[44] Y. Kuru, D. Marrocchelli, S.R. Bishop, D. Chen, B. Yildiz, H.L. Tuller, Anomalous chemical expansion behavior of $Pr_{0.2}Ce_{0.8}O_{2-\delta}$ thin films grown by pulsed laser deposition, J. Electrochem. Soc. 159 (2012) F799–F803.
[45] S. Sameshima, M. Kawaminami, Y. Hirata, Thermal expansion of rare-earth-doped ceria ceramics, J. Ceram. Soc. Jpn. 110 (2002) 597–600.
[46] R.D. Shannon, Revised effective ionic radii and systematic studies of interatomic distances in halides and chalcogenides, Acta Crystallogr. A32 (1976) 751–767.
[47] P. Hohenberg, W. Kohn, Inhomogeneous electron gas, Phys. Rev. 136 (1964) B864–B871.
[48] W. Kohn, L.J. Sham, Self-consistent equations including exchange and correlation effects, Phys. Rev. 140 (1965) A1133–A1138.
[49] G. Kresse, J. Furthmüller, Efficiency of ab-initio total energy calculations for metals and semiconductors using a plane-wave basis set, Comput. Mater. Sci. 6 (1996) 15–50.
[50] V.I. Anisimov, J. Zaanen, O.K. Andersen, Band theory and Mott insulators: Hubbard U instead of Stoner I, Phys. Rev. B 44 (1991) 943–954.
[51] S.L. Dudarev, G.A. Botton, S.Y. Savrasov, C.J. Humphreys, A.P. Sutton, Electron-energy-loss spectra and the structural stability of nickel oxide: An LSDA + U study, Phys. Rev. B 57 (1998) 1505–1509.
[52] D. Marrocchelli, S.R. Bishop, H.L. Tuller, G.W. Watson, B. Yildiz, Charge localization increases chemical expansion in cerium-based oxides, Phys. Chem. Chem. Phys. 14 (2012) 12070–12074.
[53] J.P. Perdew, K. Burke, M. Ernzerhof, Generalized gradient approximation made simple, Phys. Rev. Lett. 77 (1996) 3865–3868.
[54] P.E. Blöchl, Projector augmented-wave method, Phys. Rev. B 50 (1994) 17953–17979.
[55] G. Kresse, D. Joubert, From ultrasoft pseudopotentials to the projector augmented-wave method, Phys. Rev. B 59 (1999) 1758–1775.
[56] R. Korobko, S.K. Kim, S. Kim, S.R. Cohen, E. Wachtel, I. Lubomirsky, The role of point defects in the mechanical behavior of doped ceria probed by nano-indentation, Adv. Funct. Mater. 23 (2013) 6076–6081.
[57] H. Hayashi, M. Kanoh, C.J. Quan, H. Inaba, S. Wang, M. Dokiya, H. Tagawa, Thermal expansion of Gd-doped ceria and reduced ceria, Solid State Ionics 132 (2000) 227–233.
[58] J.S.K.-L. Gibson, S.G. Roberts, D.E.J. Armstrong, High temperature indentation of helium-implanted tungsten, Mater. Sci. Eng. A 625 (2015) 380–384.
[59] J.J. Kim, S.R. Bishop, N.J. Thompson, D. Chen, H.L. Tuller, Investigation of nonstoichiometry in oxide thin films by simultaneous in situ optical absorption and chemical capacitance measurements: Pr-doped ceria, a case study, Chem. Mater 26 (2014) 1374–1379.
[60] B.W. Sheldon, V.B. Shenoy, Space charge induced surface stresses: Implications in ceria and other ionic solids, Phys. Rev. Lett. 106 (2011) 216104.